New Hydrotalcite-like Anionic Clays Containing Zr^{4+} in the Layers: Synthesis and Physicochemical Properties

S. Velu,† D. P. Sabde, Neepa Shah, and S. Sivasanker*

Catalysis Division, National Chemical Laboratory, Pune-411 008, India

Received March 24, 1998. Revised Manuscript Received July 22, 1998

A new series of hydrotalcite (HT)-like anionic clays containing Zr^{4+} in the brucite-like layer has been synthesized by a simple coprecipitation method at constant pH. The incorporation of Zr in the layer has been investigated by various analytical methods, such as powder X-ray diffraction (PXRD), chemical analysis, FT-IR, ultraviolet−visible diffuse reflectance (UV−vis DR) spectra, and thermogravimetric analysis (TGA). The PXRD of as-synthesized samples showed that the crystallinity of the material decreased with increasing Zr content due to the distortions introduced by the incorporation of the larger cation, Zr. Thermal calcination at 723 K results in the formation of a poorly crystalline MgO phase in which some of the Zr^{4+} cations are dissolved. The crystallinity of the resulting MgO phase decreases with increasing Zr content and forms a ZrO_2 phase, in addition to the MgO phase, at higher Zr content. Calcination at higher temperatures (>1000 K) yields a mixture of MgO, $MgAl_2O_4$ spinel, and ZrO_2 phases. The UV−vis DR spectra showed that the Zr^{4+} cations are well-dispersed in both uncalcined as well as in calcined samples, similar to that in Zr-silicalites.

Introduction

Hydrotalcite (HT)-like anionic clays are a new family of interesting materials with applications as catalysts, catalyst supports, ion exchangers, and composite materials.[1−7] The structure of these compounds consists of brucite [$Mg(OH)_2$] type octahedral layers in which a part of M(II) cations are isomorphously substituted by M(III) cations. The excess positive charge of the octahedral layers resulting from this substitution is compensated for by interstitial layers built of anions such as CO_3^{2-} and crystal water. These compounds are represented by the general formula $[M(II)_{1-x}M(III)_x(OH)_2]^{x+}$ $[(A^{n-})_{x/n}\cdot yH_2O]^{x-}$, where M(II) is a divalent cation such as Mg, Cu, Ni, Co, Mn, Zn; M(III) is a trivalent cation such as Al, Fe, Cr, Ga, V,[8−10] and very recently Ru, Rh,[11] and Y;[12] A^{n-} is an interlayer anion such as CO_3^{2-}, NO_3^-, SO_4^{2-} or an organic anion such as terephthalate; and the value of x is in the range from 0.1 to 0.33. A large number of HT-like compounds with a wide variety of M(II)−M(III) cation pairs as well as M(I)−M(III) cation pairs (eg., Li−Al), with different anions in the interlayer region have been reported.[13] However, HT-like compounds with M(II)−M(IV) cation pairs such as Mg−Zr or Mg−Ti are scarcely obtained. Taylor has reported the synthesis of a Co−Ti HT-like compound employing an induced hydrolysis method[14] but without presenting the detailed physicochemical properties of the compound. In the present study we report a new series of ternary HT-like compounds containg Mg, Al, and Zr in the brucite-like layers, synthesized by employing a simple coprecipitation technique. The importance of these Zr-containing HT-like compounds stems from the fact that, similar to zeolites containing Zr (Zr-silicalites),[15−18] they could be used as catalysts for the liquid-phase hydroxylation/oxidation reactions for the synthesis of fine chemicals. Indeed, from our preliminary catalytic studies we have recently reported that these Zr-containing HT-like compounds possess excellent catalytic performance for the selective hydroxylation of phenol to catechol in the liquid phase.[19] In this paper, we report, for the first

* Author for correspondence.
† Present address: National Industrial Research Institute, Nagoya, Japan.

(1) Cavani, F.; Trifiro, F.; Vaccari, A. *Catal. Today* **1991**, 11, 173.
(2) Davis, R. J.; Derounce, E. G. *Nature* **1991**, 349, 313.
(3) Climent, M. J.; Corma, A.; Iborra, S.; Primo, J. *J. Catal.* **1995**, 151, 60.
(4) Auer, S. M.; Wandeler, R.; Gobel, U.; Baiker, A. *J. Catal.* **1997**, 169, 1.
(5) Velu, S.; Swamy, C. S. *Appl. Catal.* **1996**, 145, 141.
(6) Velu, S.; Swamy, C. S. *Catal. Lett.* **1996**, 40, 265.
(7) Li, L.; Ma, S.; Liu, X.; Yue, Y.; Hui, J.; Xu, R.; Bao, Y.; Rocha, J. *Chem. Mater.* **1996**, 8, 204.
(8) de Roy, A.; Forano, C.; Ei Malki, F.; Besse, J. P. *Expanded Clays and Other Microporous Solids*; Occelli, M. L., Robson, H. F., Eds.; Van Nostrand Reinhold: New York, 1992; p 108.
(9) Velu, S.; Swamy, C. S. *J. Mater. Sci. Lett.* **1996**, 15, 1674.
(10) Labojos, F. M.; Rives, V.; Malet, P.; Centeno, M. A.; Ulibarri, M. A. *Inorg. Chem.* **1996**, 35, 1154.
(11) Basile, F.; Basini, L.; Fornasari, G.; Gazzano, M.; Trifiro, F.; Vaccari, A. *Chem. Commun.*, **1996**, 2435.
(12) Fernandez, J. M.; Barriga, C.; Ulibarri, M. A.; Labajos, F. M.; Rives, V. *Chem. Mater.* **1997**, 9, 312.
(13) Bellotto, M.; Rebours, B.; Clause, O.; Lynch, J.; Bazin, D.; Elkaim, E. *J. Phys. Chem.* **1996**, 100, 8527.
(14) Taylor, M. M. *Clay Miner.* **1984**, 19, 591.
(15) Dongare, M. K.; Singh, P.; Moghe, P.; Ratnasamy, P. *Zeolites* **1991**, 11, 690.
(16) Rakshe, B.; Veda Ramasamy.; Ramasamy, A. V. *J. Catal.* **1996**, 163, 501.
(17) Tuel, A.; Gontier, S.; Teissier, R. *Chem. Commun.* **1996**, 651.
(18) Rakshe, B.; Veda Ramasamy.; Vetrivel, R.; Hegde, S. G.; Ramasamy, A. V. *Catal. Lett.* **1997**, 45, 41.
(19) Velu, S.; Veda Ramasamy.; Ramani, A.; Chanda, B. M.; Sivasanker, S. *Chem. Commun.* **1997**, 2107.

10.1021/cm980185x CCC: $15.00
Published on Web 10/20/1998

Table 1. Chemical Compositions, Molecular Formula, and Surface Area of MgAlZr-HT

sample	Mg:Al:Zr atomic ratio[a]	Zr/Al atomic ratio	carbon content[b] (%)	chemical formula[c]	BET surface area ($m^2\ g^{-1}$) 423 K[d]	723 K[d]
ZrHT-0	3:0.96:0.00	0.00	2.44	$Mg_6Al_2Zr_0(OH)_{16}(CO_3)_{1.12}\cdot 2.48.H_2O$	40	169
ZrHT-1	3:0.85:0.07	0.08	nd		nd[e]	202
ZrHT-2	3:0.78:0.14	0.18	2.71	$Mg_6Al_{1.6}Zr_{0.32}(OH)_{16}(CO_3)_{1.44}\cdot 2.72.H_2O$	80	241
ZrHT-3	3:0.68:0.21	0.31	2.91	$Mg_6Al_{1.36}Zr_{0.4}(OH)_{16}(CO_3)_{1.52}\cdot 2.64.H_2O$	nd	nd
ZrHT-4	3:0.67:0.33	0.49	3.01	$Mg_6Al_{1.36}Zr_{0.64}(OH)_{16}(CO_3)_{1.68}\cdot 3.20.H_2O$	68	199
ZrHT-5	3:0.57:0.37	0.65	nd		nd	nd
ZrHT-6	3:0.52:0.50	0.96	3.51	$Mg_6Al_{1.04}Zr_{1.04}(OH)_{16}(CO_3)_{2.08}\cdot 3.20.H_2O$	nd	192

[a] Determined by X-ray fluorescence spectroscopy. [b] Determined by CH microanalysis. [c] Calculated on the basis of the chemical analysis and the first weight loss in TGA. [d] Pretreatment temperature. [e] nd = not determined

time, the detailed synthesis and physicochemical characterization of these Zr-containing HT-like materials.

Experimental Section

Synthesis of Zr-Hydrotalcites. Zr-containing HT-like compounds with various Mg:Al:Zr atomic ratios were synthesized by a coprecipitation method at room temperature by reacting aqueous solutions containing a mixture of $Mg(NO_3)_2$, $Al(NO_3)_3$, and $ZrO(NO_3)_2$ salts, depending upon the Mg:Al:Zr atomic ratio and a mixture of NaOH (≈2 M solution) and Na_2CO_3 (≈0.3 M solution) at a contant pH (≈10).[20] The Mg/(Al + Zr) atomic ratio in the starting solution was kept as 3 while the Al:Zr atomic composition was varied from 0:1 to 1:0. The resulting precipitate was aged at 338 K for 30 min with magnetic stirring and then filtered, washed with distilled water several times until the pH of the filtrate was 7, and dried in an air oven at 373 K overnight.

Characterization. The chemical composition of the samples was determined by X-ray fluorescence (XRF) spectroscopy (Rigaku 3070 X-ray wavelength dispersive spectrometer). The powder X-ray diffraction (PXRD) patterns of the samples were obtained using an instrument (Rigaku, Model DMAX-III VC) equipped with a graphite crystal monochromator and Ni-filtered Cu Kα radiation (λ = 1.5418 Å). The data were collected in the 2θ range 5−70° with a scan rate of 0.5°/min for calculation of lattice parameters while a speed of 4°/min was used for obtaining the PXRD patterns. The observed interplanar d spacings were corrected using elemental Si as the internal standard. The lattice parameters were refined using two different least-squares fitting programs (HOCT and PDP11). The infrared spectra of uncalcined samples were recorded with a FT-IR (Nicolet 60 SXB model) spectrometer in the range 4000−400 cm^{-1} using KBr pellets. The same amounts of sample and KBr were used in all the pellets. The UV−vis diffuse reflectance spectra (UV−vis DRS) of all the samples were obtained using a Shimadzu UV−vis spectrophotometer (2101 PC) in the range 200−400 nm. The ^{27}Al MAS NMR spectra were recorded at room temperature in a high-resolution Bruker MSL-300 instrument operated at 78.9 MHz. The samples were loaded in a 7 mm o.d. zirconia rotor and spun at a frequency of 7 kHz while the spectra were recorded at a spectral width of 125 kHz. The chemical shift values (δ) were referenced to an aqueous solution of 1 M $Al(NO_3)_3$. The thermogravimetric analysis of these samples were carried out in a Setaram (TG/DTA 92) instrument at a scan rate of 10 K/min under an Ar atmosphere. The BET surface area of both uncalcined and calcined samples were determined by a N_2 adsorption method at 77 K using an Omnisorp 100 CX (Coulter) instrument after degassing the sample at 423 K for 8 h.

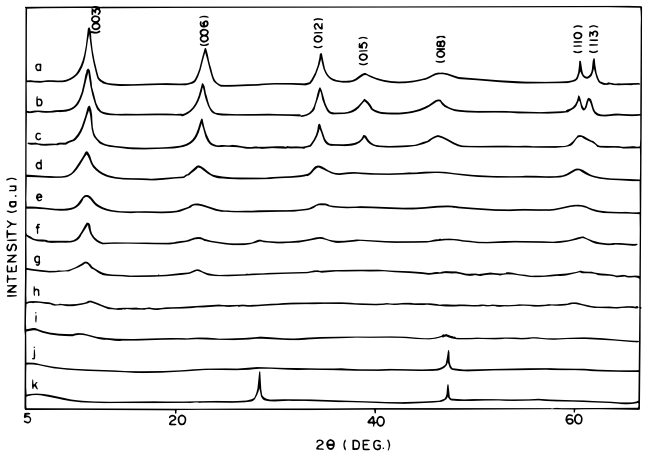

Figure 1. PXRD patterns of MgAlZr-HT: (a) ZrHT-0, (b) ZrHT-1, (c) ZrHT-2, (d) ZrHT-3, (e) ZrHT-4, (f) ZrHT-5, (g) ZrHT-6, (h) ZrHT-7, (i) ZrHT-8, (j) ZrHT-9, (k) ZrHT-10.

Results and Discussions

As-Synthesized Samples. The results of the elemental analysis of the samples prepared are included in Table 1. The Mg/(Al +Zr) atomic ratios determined from X-ray fluorescence spectroscopy are coincident, within experimental errors, with those of the starting mixed aqueous solutions and are similar (3.1 ± 0.16) for all the samples, indicating the completion of the precipitation. The PXRD patterns of these compounds with Mg:Al:Zr atomic ratio ranging from 3:1:0 to 3:0:1 are presented in Figure 1. All the samples with Zr = 0 (Mg:Al:Zr = 3:1:0) to Zr = 0.8 (Mg:Al:Zr = 3:0.2:0.8) exhibited the diffraction patterns characteristic of a HT-like structure (JCPDS file No. 22-700). However, the crystallinity of the samples decreased with increasing Zr content, probably due to the introduction of large distortions in the brucite-like layers as a result of the substitution of Al^{3+} (ionic radius 0.53 Å) by Zr^{4+} (ionic radius 0.72 Å).[21] It is also possible that the loss in crystallinity was also due to the coformation of amorphous Zr and Mg salts (such as hydroxides and hydroxy carbonates). However, in layered systems such as these, microcrystalline hydrotalcite-like phases made up of small poorly ordered sheets (X-ray amorphous) are more

(20) Velu, S.; Swamy, C. S. *Appl. Catal. A: General* **1994**, 119, 241.

(21) Shannon, R. D.; *Acta Crystallogr., Sect A* **1976**, 32, 751.

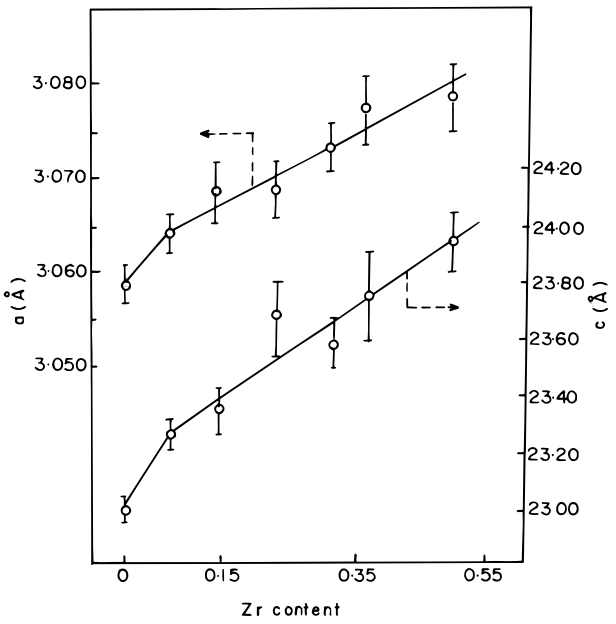

Figure 2. Variation of lattice parameters *a* and *c* with Zr content.

likely to be present in significant amounts, resulting in the overall loss of crystallinity of the samples. We, therefore, believe that Zr-containing hydrotalcite-like materials are the major component in the samples, especially so in the composition range Mg:Al:Zr = 3:1:0 (ZrHT-0) to Mg:Al:Zr = 3:0.52:0.5 (ZrHT-6), in which the diffraction peaks are intense and sharp enough to precisely determine their position. Furthermore, the binary Zr-containing HT without Al forms a poorly crystalline ZrO_2 phase, indicating that the presence of Al favors the formation of a HT-like phase. The crystallographic parameters *a* and *c* were calculated by employing least-squares refinement assuming a hexagonal crystal system for samples in the above composition range (ZrHT-0 to ZrHT-6). It can be seen from Figure 2 that both the lattice parameters *a* and *c* increase with increase in Zr content and follow the Vegard's law in the region Zr/Al = 0.08 (ZrHT-1) to 0.96 (ZrHT-6). The increase in *a* parameter can be attributed to the isomorphous substitution of Al^{3+} in the octahedral coordination by Zr^{4+} in the brucite-like layer. The *c* parameter in the HT-like system is a measure of the thickness of the brucite-like layer and the interlayer distance. It depends on several factors, such as the size of the cation, charge density, the size and the amount of the anion, its orientation, and the amount of water molecules present in the interlayer.[22,23] The thickness of the brucite-like layer would increase if a smaller cation (Al^{3+}) is substituted by a larger cation (Zr^{4+}). In the case of Mg,Al double hydroxides, the value of *c* has been found to decrease with increase in Al substitution, presumably due to an increase in the electrostatic attraction of the charged brucite-like layer with the interlayer.[1,24] In our samples, the Al-content decreases with a simultaneous increase in Zr-content. On the basis of published results,[1,24] the anticipated difference

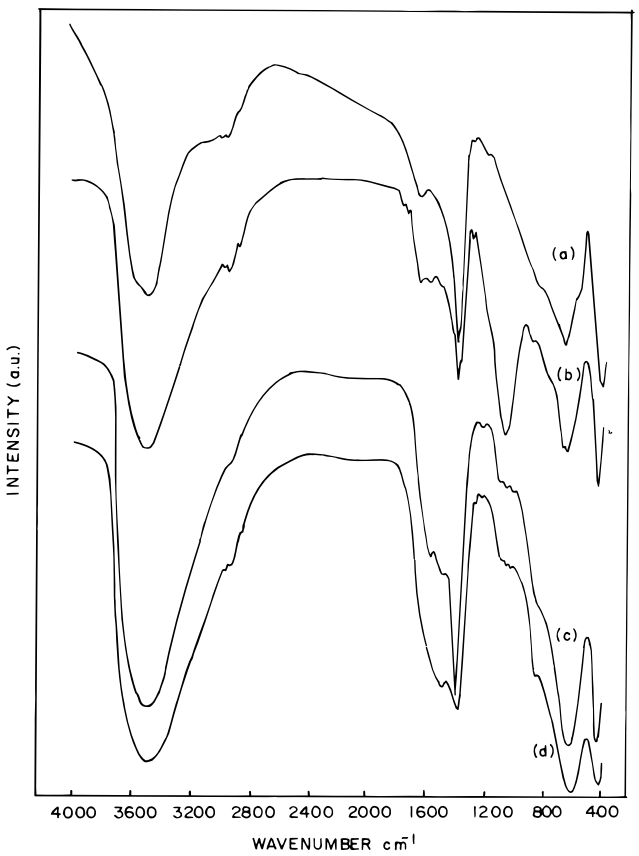

Figure 3. FT-IR spectra of MgAlZr-HT: (a) ZrHT-0, (b) ZrHT-1, (c) ZrHT-3, (d) ZrHT-6.

in the *c* value between the samples ZrHT-1 and ZrHT-6, with values of *x* of 0.22−0.13 [*x* = Al/(Al + Zr + Mg)], is less than 0.1 Å. The actual difference observed by us (Figure 2) is much larger (0.68 Å), suggesting that the increase is more due to incorporation of Zr ions and less due to the depletion of Al ions. Further, it is noticed that the *c* value of the Zr-free sample (ZrHT-0) is similar to that reported for samples of similar composition (∼23.0 Å) in the literature.[24] The increase in *c* parameter observed in our study can be attributed to many factors, such as the increase in the thickness of the brucite-like layer upon incorporation of Zr^{4+}, the decrease in the Al-content, and the accommodation of a large amount of hydrated anions in the interlayer, as evidenced from our CH micro analysis and the TG weight loss. A sharp increase in both *a* and *c* parameters is observed up to about 10% of Al^{3+} substitution by Zr^{4+}. A probable reason is that the initially added Zr^{4+} substitute for Al^{3+}, which are present at the corners of the hexagonal crystal lattice, thereby causing a sharp increase in the thickness of the brucite-like sheet.

The FTIR spectra of these samples show (Figure 3) bands characteristic of HT-like compounds containing CO_3^{2-} as the counteranions in the interlayer.[1] The incorporation of Zr^{4+} in the HT-like matrix is clearly seen from the changes in the band position (Table 2). The broad and intense band around 3500 cm^{-1} is attributed to the stretching vibration of the hydroxyl (OH) groups in the layer and of water molecules (ν_{OHstr}). The broadness of these absorption bands indicate that the OH species are hydrogen bonded. An interesting

(22) Kruissink, E. C.; von Reijen, L. L.; Ross, J. R. H. *J. Chem. Soc., Faraday Trans.* 1 **1981**, 77, 649.
(23) Yun, S. K.; Pinnavaia, T. J. *Chem. Mater.* **1995**, 7, 348.
(24) Mascolo, G. and Marino, O., *Miner. Magn.* **1980**, 43, 619.

Table 2. FT-IR Band Assignments (cm^{-1}) for MgAlZr-HT

sample	ν_{OHstr}	fwhm of ν_{OHstr}	$\nu_{HOHbend}$	ν_{CO_3r}			
				ν_1[a]	ν_2	ν_3	ν_4
ZrHT-0	3495	392	1647		871	1390	660
ZrHT-1	3486	518	1633	1062 (s)	851	1365, 1562	640
ZrHT-3	3485	549	1562	1041 (w)	851	1379, 1485	604
ZrHT-6	3457	612	1555	1027 (w)	844	1386, 1485	604

[a] s, strong band; w, weak band.

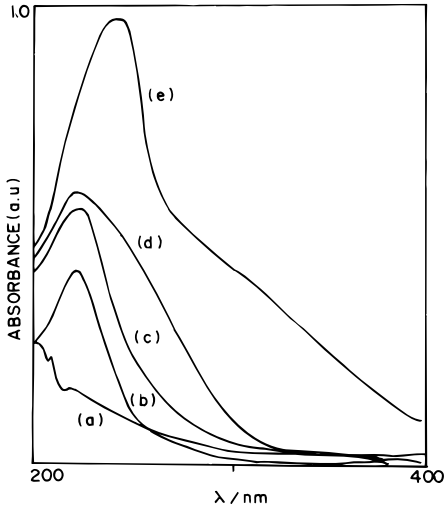

Figure 4. UV−vis DR spectra of MgAlZr-HT: (a) ZrHT-1, (b) ZrHT-3, (c) ZrHT-5, (d) ZrHT-8, (e) ZrO_2.

observation noticed in the FT-IR of these compounds is that the fwhm values of ν_{OHstr} increase gradually with increasing Zr content (Table 2). This can be attributed to the increase in the cation distribution[24] due to the incorporation of Zr^{4+} in the brucite-like layer. This is in accordance with the earlier results in which the fwhm values of ν_{OHstr} have been found to depend on the nature of the interlayer anions.[25,26] The medium intensity absorption band around 1600 cm^{-1} is due to the deformation (HOH bending) mode of water molecules ($\nu_{HOHbend}$). The band positions of both ν_{OHstr} and $\nu_{HOHbend}$ are shifted toward lower wavenumbers when the Zr content is increased, presumably due to the lowering of the electron density of the OH groups coordinated with Zr^{4+} cations. The weak absorption bands around 2900 cm^{-1}, appearing as shoulders, are attributed to the water molecules hydrogen bonded to CO_3^{2-} anions in the interlayer. A sharp and intense band appears at 1390 cm^{-1} for the sample ZrHT-0 and is ascribed to the ν_3 stretching vibration of the CO_3^{2-} ion. However, upon incorporation of Zr, an additional band (weak) appears at 1562 cm^{-1} for ZrHT-1 and at 1485 cm^{-1} for ZrHT-3 and ZrHT-6 (Figure 3, Table 2) and also the IR-forbidden ν_1 stretching of CO_3^{2-} occurs around 1020−1060 cm^{-1}. Similar results were also observed for other HT-like materials containing larger cations such as Y^{3+} or Cr^{3+} in the brucite layer and are attributed to the partial loss of symmetry of the CO_3^{2-} ion in the restricted interlayer.[12] Hence it can be stated that the symmetry of the CO_3^{2-} ion (D_{3h}) in the interlayer is perturbed upon incorporation of Zr in the layer. The

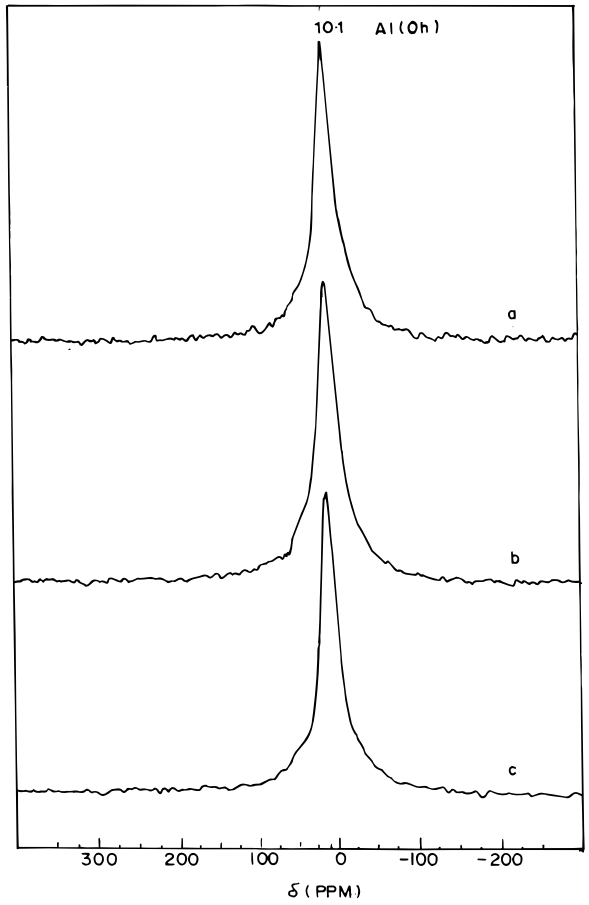

Figure 5. ^{27}Al MAS NMR spectra of MgAlZr-HT: (a) ZrHT-0, (b) ZrHT-1, (c) ZrHT-3.

ν_2 and ν_4 bands of CO_3^{2-} which appear at 870 and 650 cm^{-1} in ZrHT-0 are also shifted toward lower frequency. The other bands observed below 1000 cm^{-1} are generally attributed to the vibration of M−O, M−O−M and O−M−O bonds in the brucite-like lattice.

The dispersion of Zr in the HT matrix was studied by UV−vis diffuse reflectance spectroscopy (UV−vis DRS). It can be seen from Figure 4 that all the samples exhibit a single narrow band around 210 nm which is attributed to charge-transfer involving isolated Zr^{4+} species.[16,17] This electronic transition is clearly distinguishable from that of pure ZrO_2, which shows strong absorption bands around 240 and 320 nm (Figure 4, curve e). These results demonstrate the absence of any ZrO_2 species within the sample and indicate that the Zr^{4+} cations are wel-dispersed in the HT framework, similar to that in Zr-silicalites.[16−18]

The nature of coordination of Al in these Zr-containg HT-like compounds has been studied by ^{27}Al MAS NMR spectroscopy. Figure 5 shows the ^{27}Al MAS NMR spectra of some of these samples. The indicated chemi-

(25) Hernandez-Moreno, M. J.; Ulibarri, M. A.; Rendon, J. L.; Serna, C. *J. Phys. Chem. Mineral.* **1985**, 12, 34.
(26) Velu, S.; Ramkumar, V.; Narayanan, A.; Swamy, C. S. *J. Mater. Sci.* **1997**, 32, 957.

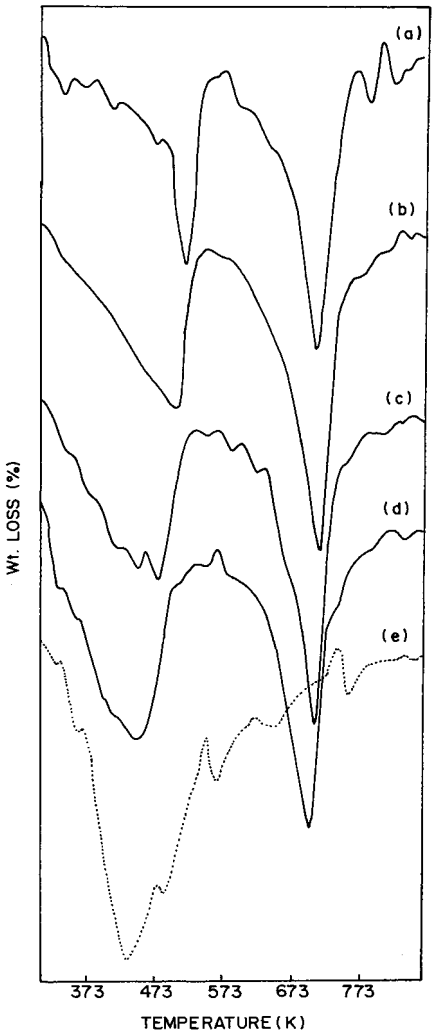

Figure 6. DTGA traces of MgAlZr-HT: (a) ZrHT-0, (b) ZrHT-1, (c) ZrHT-3, (d) ZrHT-6, (e) ZrHT-10.

cal shifts are observed values without second-order quadruple corrections. It can be seen that these synthetic samples show a single resonance around 10 ppm, indicating that all the Al^{3+} ions are present in octahedral coordination and there is not much influence on chemical shift with respect to Zr content in the sample.

The thermogravimetric analysis (TGA) of hydrotalcite-like compounds generally shows two stages of the weight loss process. Figure 6 shows the differential curves of TGA (DTGA) of some of the MgAlZr-HT. All the samples except ZrHT-10 exhibit two major weight loss processes characteristic of HT-like compounds having layered structures.[1,12] The first weight loss (T_1) occurring in the temperature range 423−523 K is attributed to the removal of interlayer water. The second weight loss (T_2) observed around 623−723 K is due to the removal of structural water and CO_2 from the decomposition of CO_3^{2-} ions in the interlayer. It is interesting to note that the incorporation of Zr in the HT-like lattice results in the broadening of the T_1 process (curves b−d), indicating that the weight loss is associated with some complicated process, probably due to the removal of large amounts of physisorbed water and CO_3^{2-} ions. In addition, the peak temperatures for both processes are shifted toward lower temperature with increasing Zr content (e.g., ZrHT-0; T_1 = 514 K, T_2 = 703 K: ZrHT-6; T_1 = 436 K, T_2 = 683 K). These results clearly indicate that the incorporation of Zr in the HT lattice facilitates the decomposition process due to the weakening of the interaction between the brucite-like layer and the interlayer (cf. PXRD results, Figure 2). A net weight loss of around 40−50% has been recorded in the TGA up to 873 K in these samples. From the weight loss recorded for the T_1 process (373−523 K) and the results of chemical compositions as determined from the XRF and CH analysis, the chemical formula of the compounds are derived and are presented in Table 1. The DTG diagram of ZrHT-10, without Al, shows (curve e) a single broad weight loss process, probably due to the decomposition of some amorphous hydroxycarbonates since the PXRD of this sample shows a poorly crystalline ZrO_2 phase (Figure 1, curve k). These differences in the thermogravimetric study also indicate the incorporation of Zr in the lattice.

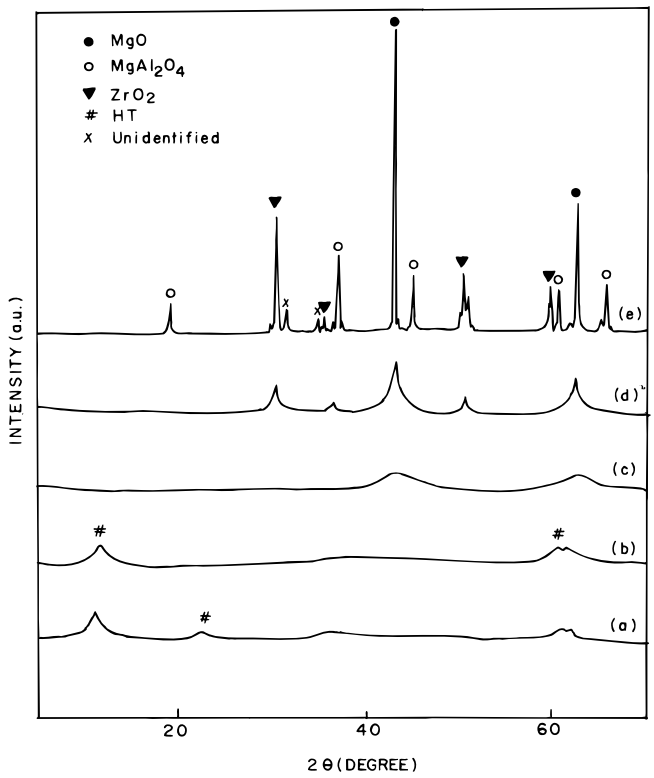

Figure 7. PXRD patterns of ZrHT-3 calcined at (a) 423 K, (b) 573 K, (c) 723 K, (d) 1073 K, and (e) 1473 K for 4 h.

Calcined Products. Thermal calcination of HT-like compounds results in the decomposition of the layer structure and various metastable phases are formed, depending on the calcination temperature. The determination of crystalline phases formed during calcination at various temperatures is useful to understand the thermal stability of the compounds. Figure 7 shows the PXRD patterns of ZrHT-3 calcined at various temperatures for 4 h in air. It can be seen that at 423 K, all the peaks corresponding to HT are retained with reduced intensities (compare Figure 1, curve d and Figure 7, curve a). At 573 K, the peak corresponding to (006) completely disappears while the (003) diffraction line is shifted toward a higher 2θ value (lower interlayer spacing) due to the removal of interlayer water molecules. These results indicate that the HT-like structure in these compounds survives up to at least

573 K. However, at 723 K, the layered structure completely collapses due to the removal of structural water and CO_2 from the interlayer. The evolution of these gases during calcination makes craters on the surface, and hence the surface area increases from around 40 $m^2\ g^{-1}$ for the uncalcined samples to about 200 $m^2\ g^{-1}$ for samples calcined at 723 K (Table 1). The material at this temperature is referred to as a poorly crystallized MgO, whose crystallinity increases with further increase in calcination temperature to 1073 K. At this temperature, in addition to MgO, weak diffraction lines are recorded which are attributed to the formation of $MgAl_2O_4$ spinel and ZrO_2 phases. At 1473 K, the intensity of all these diffraction lines increase to form well-defined crystalline phases.

It has been reported[26,27] that in the case of MgAl−HT, calcination above 900 K yields a mixture of MgO and $MgAl_2O_4$ phases while a mixture of MgO, $MgAl_2O_4$, and RuO_2 phases are reported to be formed in a ternary MgAlRu−HT.[11] On the other hand, Fernandez et al.[12] noticed a mixture of MgO, $MgAl_2O_4$, and $Al_2Y_4O_9$ phases during calcination of MgAlY−HT at 1273 K. However, in the present study, we have not noticed any Zr-containing phase other than ZrO_2, even at 1473 K.

The ^{27}Al MAS NMR spectra of uncalcined samples showed (Figure 4) a single resonance around 10 ppm, indicating that all the Al are present in octahedral coordination. However, upon calcination at 723 K, the destruction of the brucite-like layer causes the appearance of an additional resonance around 75 ppm (Figure 8), attributed to the transformation of the coordination of Al from octahedral (Oh) to tetrahedral (Td).[28] In addition, a shift in Al (Oh) resonance from around 10 ppm to around 15 ppm is observed (compare Figure 4, curve b and Figure 8, curve b), indicating a change in the environment of Al, possibly due to the formation of solid solutions in which Al^{3+} ions mainly occupy the sites in MgO lattice. Further increase in the calcination temperature to 1073 and 1473 K results in an increase in the intensity of the Al (Td) resonance, probably because of the formation of $MgAl_2O_4$ spinel phase in addition to the MgO phase in this temperature range, as evidenced from PXRD (Figure 7). The formation of the $MgAl_2O_4$ spinel phase also causes a gradual shift in both Al (Td) and Al (Oh) resonance peaks toward lower chemical shift.

On the basis of the results obtained from TGA, PXRD, and ^{27}Al MAS NMR spectra, the following reaction scheme can be proposed for the decomposition of MgAlZr-HT at various temperatures.

Among the phases formed during the calcination of HT-like materials, the one formed around 723 K is of particular interest, since in many cases the product formed at this calcination temperature is used as catalyst for many industrially important reactions.[1−6] Hence we have studied, in detail, the nature of the products formed at 723 K by PXRD and UV−vis DRS. Figure 9 shows the PXRD patterns of various MgAlZr-HT calcined at 723 K for 4 h. It can be seen that a poorly crystalline MgO phase is obtained in all cases

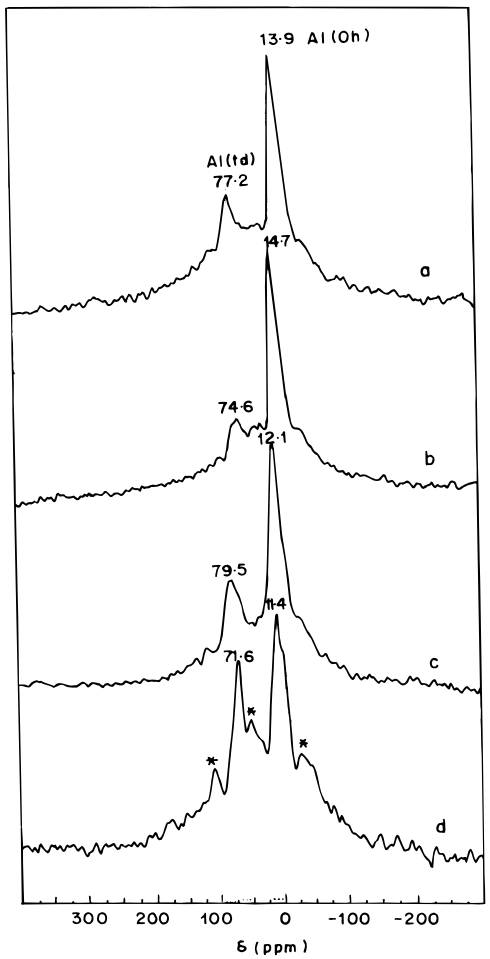

Figure 8. ^{27}Al MAS NMR spectra of (a) ZrHT-1 calcined at 723 K and (b) ZrHT-3 calcined at 723 K, (c) 1073 K, and (d) 1473 K. *Spinning sidebands

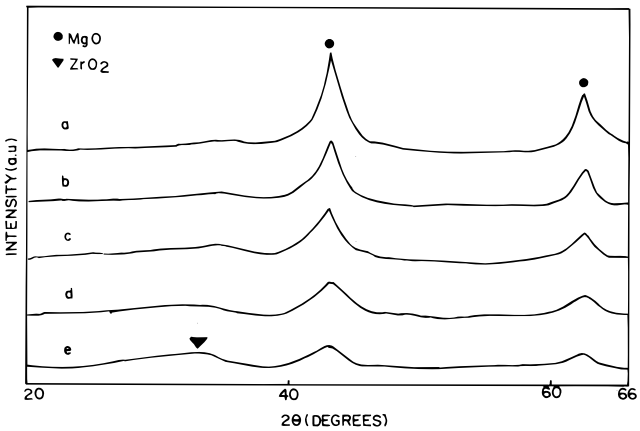

Figure 9. PXRD patterns of MgAlZr-HT calcined at 723 K for 4 h: (a) ZrHT-0, (b) ZrHT-1, (c) ZrHT-3, (d) ZrHT-5, (e) ZrHT-8.

and the crystallinity decreases further with increasing Zr content. In addition, the formation of a separate ZrO_2 phase (poorly crystalline) is evidenced in ZrHT-7.

It has been reported by several authors[1,3,20,26] that the thermal decomposition of MgAl-HT around 723 K yields a poorly crystalline phase corresponding to MgO whose lattice constant *a* is less than that of pure MgO and has been attributed to the dissolution of a small amount of Al^{3+} in the MgO lattice to form solid solutions. The chemical composition of the resulting solid solution is

(27) Arco, M.; Rives, V.; Trujillano, R.; Malet, P. *J. Mater. Chem.* **1996**, 6, 1419.
(28) Mackenzie, K. J. D.; Meinhold, R. H.; Sherriff, B. L.; Zhixu. *J. Mater. Chem.* **1993**, 3, 1263.

$$Mg_6Al_{2-x}Zr_x(OH)_{16}\,[(x+2)/2]CO_3\ n.H_2$$

$$\downarrow -\ n.H_2O,\ \sim 573\ K$$

$$Mg_6Al_{2-x}Zr_x(OH)_{16}\,[(x+2)/2]CO_3$$

$$\downarrow -\ H_2O,\ -\ CO_2,\ \sim 723\ K$$

$$(MgO)^{\#} + (XAP)^{*}$$

$$\downarrow \sim 1073\ K$$

$$MgO + MgAl_2O_4 + ZrO_2$$

$(MgO)^{\#}$ = solid solution

$(XAP)^{*}$ = X-ray amorphous phase

given by the formula $Mg_{(1-x)/(2+x)}Al_{2x/(2+x)}\square_{x/(2+x)}O$, where $\square$ is a cation vacancy created due to the dissolution of some of the Al in the MgO lattice.[29] In the present study, since the PXRD lines are very broad and less intense, an accurate determination of the lattice parameters of the calcined products has not been possible. Hence, we have calculated only the *d*(200) values (the most intense peak) of the resulting MgO phase for all the samples and compared them. It can be seen from Figure 10 that the *d*(200) value increases with increasing Zr content and follows Vegard's law only in the composition range Zr/Al = 0−0.65. This result indicates that a portion of the Al^{3+} (ionic radius 0.53 Å) in the above Mg−Al−O solid solution is isomorphously substituted by Zr^{4+} (ionic radius 0.72 Å) to form Mg−Al−Zr−O solid solution similar to the composition described above. The decrease in *d*(200) values at higher Zr content could be attributed to the segregation of Zr^{4+} at the surface to form a separate ZrO_2 phase, as evidenced from PXRD (curve e).

The UV−vis DR spectra of these samples calcined at 723 K for 4 h (Figure 11) are similar to those of the uncalcined samples (Figure 5) exhibiting a single narrow band around 210 nm. However, the absorbance maxima are more intense and sharper than those of the uncalcined samples, indicating that the Zr^{4+} cations are well-dispersed in calcined samples. For comparison, the UV−vis DR spectra of pure ZrO_2 (curve e) and a physical mixture of ZrHT-0 calcined at 723 K (ZrCHT-0) + ZrO_2 (curve - - - -) were also recorded. It can be seen that the addition of about 15−20 wt % of ZrO_2 to ZrCHT-0 creates absorbance bands similar to those of pure ZrO_2 (strong absorbance bands around 240 and 320 nm). The absence of such absorbance bands in the calcined (at 723 K) ZrHT samples indicates the absence of the ZrO_2 phase. In the case of ZrCHT-8, the tailing of the absorbance bands in the higher wavelength region (curve d) indicates the presence of at least a small amount of ZrO_2 in the sample, as evidenced by PXRD (Figure 9, curve e). Hence, on the basis of the results obtained from PXRD and UV−vis DR spectra, it can be concluded that thermal calcination of Zr-containing HT

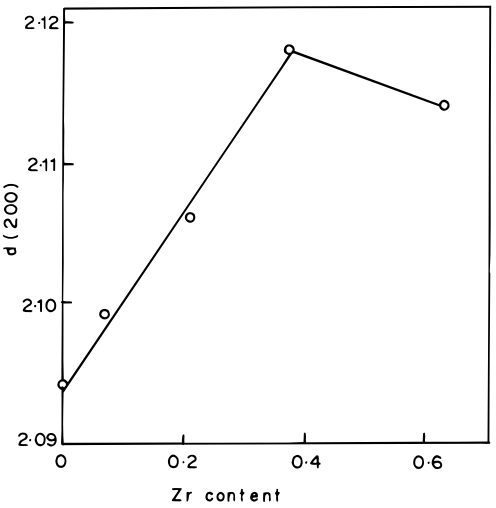

Figure 10. Variation of lattice parameter *d*(200) of the MgO phase with Zr content.

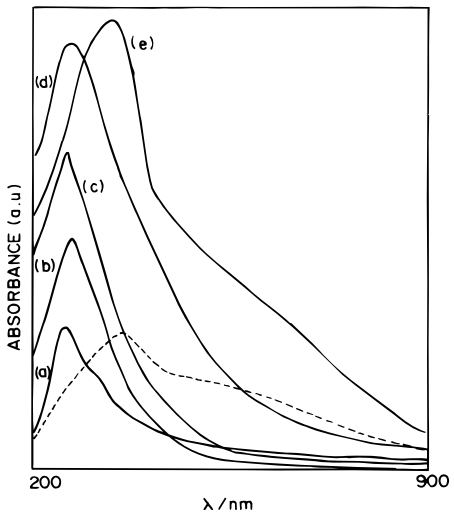

Figure 11. UV−vis DR spectra of MgAlZr-HT calcined at 723 K for 4 h: (a) ZrHT-1, (b) ZrHT-3, (c) ZrHT-5, (d) ZrHT-8, (e) ZrO_2, (- - -) ZrHT-0 + ZrO_2 (physical mixture).

at 723 K forms a poorly crystalline MgO phase in which the Zr^{4+} cations are well dispersed in the matrix. The crystallinity of the resulting MgO phase decreases with an increase in Zr content up to around 15 atom % [of Zr/(Mg + Al + Zr)].

Conclusions

Pure and crystalline Mg−Al−Zr HT-like compounds with Mg:Al:Zr = 3:0:0.96 to 3:0.52:0.5 can be easily synthesized by a simple coprecipitation method. The crystallinity of the material decreases with an increase in Zr content. The incorporation of Zr in the brucite-like layer reduces the symmetry of the CO_3^{2-} anion in the interlayer and also the thermal stability of the material. Thermal calcination at 723 K offers a poorly crystalline phase corresponding to MgO in which a part of the Zr^{4+} cations are dissolved along with Al^{3+} cations to form a solid solution containing the cation vacancy. Calcination at higher temperature (>1000 K) yields a mixture of MgO, $MgAl_2O_4$ spinel, and ZrO_2 phases. The Zr^{4+} cations are well-dispersed in both uncalcined as well as in calcined samples (at 723 K) and the resulting

(29) Constantino, V. R. L.; Pinnavaia, T. J. *Catal. Lett.* **1994**, 23, 361.

Zr-HT-like compounds are expected to serve as efficient catalysts in liquid-phase hydroxylation/oxidation reactions.

Acknowledgment. The authors are grateful to Dr. (Mrs.) Veda Ramaswamy and Dr. P. R. Rajamohanan, NCL, Pune for PXRD and ^{27}Al MAS NMR studies, respectively. S.V, D.P.S, and N.S. thank the Council of Scientific and Industrial Research, New Delhi, India, for research fellowships.

CM980185X